# Confining bond rearrangement in the random center vortex model

Derar Altarawneh,[1,2,*] Roman Höllwieser,[1,3,†] and Michael Engelhardt[1,‡]

[1]*Department of Physics, New Mexico State University, PO Box 30001, Las Cruces,*
*New Mexico 88003-8001, USA*
[2]*Department of Applied Physics, Tafila Technical University, Tafila 66110, Jordan*
[3]*Institute of Atomic and Subatomic Physics, Nuclear Physics Department,*
*Vienna University of Technology, Operngasse 9, 1040 Vienna, Austria*

We present static meson-meson and baryon-antibaryon potentials in $Z(2)$ and $Z(3)$ random center vortex models for the infrared sector of Yang-Mills theory, i.e., hypercubic lattice models of random vortex world surfaces. In particular, we calculate multiple Polyakov loop correlators corresponding to static meson-meson or baryon-antibaryon configurations in a center vortex background and observe that their expectation values follow the minimal area law, displaying bond rearrangement behavior, a characteristic expected for the confining dynamics of the strong interaction. The static meson-meson and baryon-antibaryon potentials are compared with theoretical predictions and lattice QCD simulations.

## I. INTRODUCTION

Center vortices [1–6] are closed tubes of quantized chromomagnetic flux which spontaneously condense in the vacuum, giving rise to the nonperturbative phenomena which characterize the infrared sector of strong interaction physics, namely, quark confinement, the spontaneous breaking of chiral symmetry ($\chi$SB) and the axial $U_A(1)$ anomaly.

The vortex model of confinement has been buttressed by a multitude of studies, in lattice Yang-Mills theory (see, e.g., [7–15]), within the infrared effective model of center vortices under investigation here [16–24] and another infrared model of random vortex lines in continuous three-dimensional (3D) space-time [25,26] and also by theoretical effective model calculations, e.g., [27–30]. The physical motivation for the vortex picture can be seen from the Wilson loop criterion of confinement; i.e., the expectation value of the Wilson loop has to follow an area law in the confined phase. The vortex model deduces the area law from independent vortex piercings of the Wilson loop, which can be interpreted as crossings of the static electric flux tube and moving closed magnetic flux. The area law follows from fluctuations in the number of vortices piercing a Wilson loop, and the deconfinement transition in the center vortex picture takes the guise of a percolation transition [13,16].

Numerical simulations indicate further that vortices are responsible for $\chi$SB as well [18,24,31–52]. Removal of center vortices restores chiral symmetry [31]. A dense vortex vacuum gives rise to a finite density of Dirac operator near-zero modes (see also [53,54]), hence a finite chiral condensate via the Banks-Casher relation [55], spontaneously breaking chiral symmetry. More than one concrete mechanism may be at play in generating the near-zero mode spectrum. On the one hand, center vortices give rise to lumps of topological charge through (self-)intersection and writhe, as well as through their color structure. These attract Dirac zero modes, which can interact to generate the near-zero mode spectrum in a manner reminiscent of the instanton liquid model, as studied in [46], where the close analogy between specific spherical vortex configurations and instantons was noted. On the other hand, even in the absence of would-be zero modes generated by topological charge lumps, the random interactions of quarks with the vortex background may be strong enough to smear the free quark dispersion relation such that the spectral density of the Dirac operator becomes nonzero near zero eigenvalue [18]. As vortices modify their percolation behavior at the deconfinement transition, chiral symmetry is restored [18].

A recent study of double-winding Wilson loops [56] further favors the center vortex degrees of freedom as the dominating fluctuations in the QCD vacuum. The spatial distribution of center vortex fields not only gives the area law falloff for simple Wilson loops but also shows the correct difference of areas' behavior for double-winding Wilson loops, in contrast to other confining gluonic field fluctuations. Further details, including an outlook on the relation of the vortex picture to other models of the strong interaction vacuum, can be found in the reviews [57,58].

In the present work we revisit the random vortex world-surface model, which will be introduced in the next section along with its main achievements, to measure static meson-meson and baryon-antibaryon correlators, as specified in Sec. III together with simulation details and the exponential error reduction method. In these correlators, we observe bond rearrangement behavior as the relative positions of the static quarks are varied, in accordance with a strict minimal

[*]derar@nmsu.edu
[†]hroman@kph.tuwien.ac.at
[‡]engel@nmsu.edu

area law, operative already at finite separations. The confining bonds within each mesonic or baryonic cluster appear to be fully saturating, with no residual interactions between clusters. Thus, cluster separation occurs not only asymptotically, where it would be expected on general grounds, but already at intermediate distances. We present these results in Sec. IV and furthermore compare them with theoretical expectations and measurements in lattice QCD. We draw our conclusions in Sec. V.

## II. RANDOM VORTEX WORLD-SURFACE MODEL

The random center vortex world-surface model [16,19] describes the infrared gluonic dynamics in the strong interaction vacuum in terms of collective degrees of freedom called center vortices, which represent random closed lines of quantized chromomagnetic flux. In terms of field configurations in four-dimensional (Euclidean) space-time, these correspond to an ensemble of closed random world surfaces. The concrete implementation of this model ensemble studied in the following employs a hypercubic lattice, on which the random surfaces are composed of elementary lattice squares. The ensemble is governed by an action related to surface curvature[1]: If two of the aforementioned elementary squares composing a vortex surface share a lattice link while lying in different lattice planes, an action increment $c$ is incurred. This can be written formally in terms of a sum over lattice links,

$$
\begin{aligned}
S[q] = c \sum_x \sum_\mu &\left[ \sum_{\substack{\nu<\lambda \\ \nu\neq\mu,\lambda\neq\mu}} (|q_{\mu\nu}(x)q_{\mu\lambda}(x)| \right. \\
&+ |q_{\mu\nu}(x)q_{\mu\lambda}(x-e_\lambda)| + |q_{\mu\nu}(x-e_\nu)q_{\mu\lambda}(x)| \\
&+ \left. |q_{\mu\nu}(x-e_\nu)q_{\mu\lambda}(x-e_\lambda)|) \right] \\
= \frac{c}{2} \sum_x \sum_\mu &\left[ \left[ \sum_{\nu\neq\mu}(|q_{\mu\nu}(x)| + |q_{\mu\nu}(x-e_\nu)|) \right]^2 \right. \\
&- \left. \sum_{\nu\neq\mu}[|q_{\mu\nu}(x)| + |q_{\mu\nu}(x-e_\nu)|]^2 \right],
\end{aligned}
\tag{1}
$$

---

[1]A systematic gradient expansion of the vortex world-surface action starts with a Nambu-Goto term (proportional to the world-surface area), followed by a curvature term. The effects of these terms are correlated; configurations with more area will generically also contain more curvature. In [16,19], the two-dimensional plane of coupling constants corresponding to the aforementioned two action terms was explored, and it was indeed found that the terms can to a certain extent be traded off against one another. Lines of approximately constant physics were identified, on which characteristics of $SU(2)$ and $SU(3)$ Yang-Mills theory are reproduced. These lines of constant physics contain points on which the Nambu-Goto term vanishes (but do not include points on which the curvature term vanishes). Consequently, these points in the coupling constant plane were adopted as the simplest realization of the vortex world-surface model consistent with the confinement characteristics of Yang-Mills theory.

where $q_{\mu\nu}(x)$ specifies the chromomagnetic flux associated with the elementary square that extends from the site $x$ into the positive $\mu$ and $\nu$ directions. The variables $q_{\mu\nu}(x)$ take three values, $q_{\mu\nu}(x) \in \{-1, 0, 1\}$; the value 0 means that the elementary square is not part of a vortex surface, whereas nonzero quantized flux carried by the vortices is encoded in the other values $\pm 1$. The sign of $q_{\mu\nu}(x)$ corresponds to the orientation of the vortex flux, implying the relation $q_{\nu\mu}(x) = -q_{\mu\nu}(x)$, as will be clear from the characterization of vortex flux by its effect on Wilson loops circumscribing it, given in the next section. For the purpose of evaluating Wilson loops, in the $SU(2)$ case it will be seen that there is no physical distinction between the $\pm 1$ fluxes, and one could equivalently adopt a scheme in which $SU(2)$ elementary vortex squares only take the value $+1$; for consistency of notation, this option is not employed here. In the $SU(3)$ case, by contrast, the $\pm 1$ fluxes have physically distinct effects on Wilson loops, and one must keep track of the orientation of vortex flux.

Vortex flux is subject to the Bianchi identity; i.e., it is continuous modulo $2\pi$, i.e., modulo Dirac strings [17–19]. Vortex world surfaces therefore are closed, as already mentioned above. Nevertheless, in the $SU(3)$ case, vortex branchings are allowed; flux continuity is respected when a $\pm 1$ vortex splits into two $\mp 1$ vortices, and vice versa. In the $SU(2)$ case, such branchings do not occur; there is really only one physical vortex flux, and the distinction between $+1$ and $-1$ flux is purely formal for present purposes, as already noted above. This corresponds to there being only one nontrivial center element in the $SU(2)$ group. These constraints stemming from continuity of flux must be respected in the generation of the random surface ensemble; in practice, this is achieved by performing Monte Carlo updates on all six squares making up the surface of an arbitrary elementary three-dimensional cube in the lattice simultaneously [19]. Essentially, the continuous flux of a vortex of the shape of the elementary cube surface is superposed onto the previously present flux.

This infrared effective model of strong interaction dynamics has been explored extensively, ascertaining the reach of such a description of the QCD vacuum in terms of vortex degrees of freedom with their simplified effective action. Initial studies focused on the $SU(2)$ gauge group; the random vortex world-surface model was seen to allow for both a low-temperature confining as well as a high-temperature deconfined phase [16], which are separated by a second-order phase transition [19]. The spatial string tension in the deconfined phase [16], the topological susceptibility [17] and the (quenched) chiral condensate [18] are predicted in quantitative agreement with $SU(2)$ lattice Yang-Mills theory. Extending the model to $SU(3)$ color, a weakly first-order deconfinement phase transition [19] was found, and confirmed by investigating the vortex free energy [20]. The baryonic static potential exhibits a $Y$ law [21], and also the $SU(3)$ topological susceptibility was

evaluated [24]. Further gauge groups were studied in order to better understand the systematics of competing confinement mechanisms [59], including $SU(4)$ color [22] and $Sp(2)$ color [23]. It was seen that the vortex picture is sufficiently flexible to account for the confinement properties associated with various gauge symmetries, provided the effective dynamics are suitably tailored; in general, one must employ more complex effective actions than the simple curvature action (1) describing the $SU(2)$ and $SU(3)$ cases. The present work revisits the latter, widening the scope from the simplest confinement properties studied previously, as described above, to more complex static meson-meson and baryon-antibaryon correlators.

## III. OBSERVABLES AND EXPONENTIAL NOISE REDUCTION

Our objective is to evaluate expectation values of multiple Polyakov loop operators in a center vortex background. Studies of quantities of this type have also been suggested in [60]. Generally, Wilson loops[2] are influenced by the quantized chromomagnetic flux carried by center vortices in a characteristic fashion: For an arbitrary area spanning a given Wilson loop (the choice of area being immaterial owing to flux continuity), each time the area is pierced by a vortex world surface,[3] the Wilson loop is multiplied by a phase corresponding to a nontrivial center element of the gauge group. Specifically, in the $SU(2)$ color case, each piercing contributes a phase $(-1) = \exp(\pm i\pi)$, whereas in the $SU(3)$ color case, two distinct phase factors are possible, corresponding to the two possible quantized vortex fluxes, namely, $\exp(\pm i2\pi/3)$. Note, thus, that there is no physical distinction in the $SU(2)$ case between the two orientations of vortex flux, as already mentioned further above. To cast these properties into precise language, in terms of the variables $q_{\mu\nu}(x)$, consider evaluating an elementary Wilson loop, i.e., the plaquette $U_{\kappa\lambda}(y)$, starting at the (dual) lattice site $y$, integrating first into the positive $\kappa$ direction and then into the positive $\lambda$ direction, and continuing around the plaquette. This plaquette is pierced (only) by the lattice elementary square $q_{\mu\nu}(x)$, with the indices $\kappa$, $\lambda$, $\mu$, $\nu$ spanning all four space-time dimensions and $x = y + (\vec{e}_\kappa + \vec{e}_\lambda - \vec{e}_\mu - \vec{e}_\nu)a/2$, where $a$ denotes the lattice spacing. Thus, $U_{\kappa\lambda}(y)$ is determined exclusively by $q_{\mu\nu}(x)$ as

$$U_{\kappa\lambda}(y) = \exp(i\pi/N \cdot \epsilon_{\kappa\lambda\mu\nu} q_{\mu\nu}(x)), \qquad (2)$$

where $N$ is the number of colors and the usual Euclidean summation convention over Greek indices applies. An arbitrary Wilson loop can be evaluated [21] by finding a tiling of that loop by a set of plaquettes, and multiplying the values (2) of those plaquettes in the given vortex configuration.

To probe static meson-meson potentials, one measures the correlator of two (flat) Wilson loops of size $R \times T$, i.e., the quark and antiquark in each static meson are separated by a distance $R$ in a spatial direction and are propagating in time direction, with distance $D$ between the two mesons in an orthogonal spatial direction. To probe static baryon-antibaryon potentials, the spatial setup depicted in Fig. 1(b) was adopted: Two Wilson loops of size $R \times T$ (static mesons) with opposite orientations are combined to construct a propagating static linear baryon; i.e., the three quarks in the baryon lie equidistantly along one line with total extent $2R$. This pair of Wilson loops is then again correlated with a mirrored pair of loops for the antibaryon at distance $D$. A comment is in order concerning this particular choice for the spatial arrangement of the quarks, which is owed to computational simplicity. A realistic baryon, of course, is not described by any particular static arrangement of quarks, but by a wave function which features a finite probability density for linear, triangular, and a continuum of other spatial arrangements of the quarks (presumably, approximately triangular arrangements are somewhat more likely than approximately linear ones). Studying all these possibilities in a representative manner lies beyond the scope of this work. No particular choice will adequately represent an actual baryon; this is not the intent of the present study. Instead, the focus lies on the gluonic dynamics alone, namely, on the confining bond rearrangements given a collection of quarks. To address this question, a particular spatial arrangement is selected from among the continuum which occurs in a baryon. The linear arrangement has the advantage that all bonds occur along lattice axes, and therefore the resulting data do not have to be disentangled with respect to, e.g., effects of rotational symmetry breaking when bonds do not lie along axes. As already noted above, a detailed study of the baryonic $Y$ law, including off-axis bonds, was carried out in [21].

In practice, in the present work, the Wilson loops were chosen to extend over the entire temporal extent of the lattice, in which case the correlators described above take the form of multiple Polyakov loop correlators. Static meson-meson correlators are obtained from four, static baryon-antibaryon correlators from six Polyakov loops; see Fig. 1.

To reduce the numerical noise contaminating the mesonic and baryonic Polyakov loop correlator measurements as far as possible, the noise reduction technique introduced by Lüscher and Weisz [61] was employed, adapted to the random center vortex world-surface model [21].

---

[2]A correlator of two Polyakov loops can be viewed as a special case of a Wilson loop, extending along the entire temporal direction of the lattice; note that no path ordering issues arise in the present case, owing to the Abelian character of the $Z(N)$ vortex configurations.

[3]Wilson loops are defined on the lattice which is dual to the one on which the vortex world surfaces are defined, i.e., on a lattice shifted by the vector $(a/2, a/2, a/2, a/2)$, where $a$ is the lattice spacing. Consequently, the notion of a Wilson loop area being pierced by a vortex world surface is unambiguous.
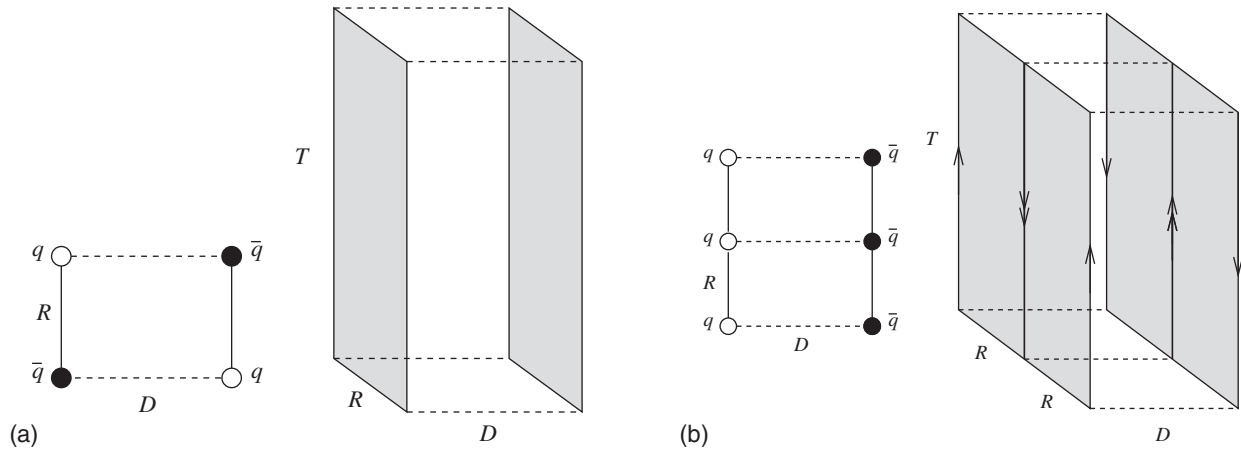
FIG. 1.   Polyakov loop setups for static (a) meson and (b) baryon correlators.

As noted in conjunction with (1), the vortex world-surface action takes the form of a sum over contributions associated with lattice links. The contribution at each link couples only elementary squares attached to the link. The action can thus be decomposed in the form

$$S[q] \equiv S[q^t, q^s] = S^t[q^t] + \sum_i S^i[q^t, q_i^s], \qquad (3)$$

where the set of variables $q^t$ represents all elementary squares that extend into the time and one space direction, whereas the set of variables $q_i^s$ represents the elementary squares extending into two spatial directions at fixed lattice time $i$. The $S^i$ piece of the action thus contains the sum over spatial links at lattice time $i$, and $S^t$ contains the sum over all temporal links. The constraint of continuity of flux can be treated in an analogous manner; it is a constraint that must be satisfied at each lattice link separately [21], and in each case involves precisely the elementary squares attached to the link in question. The constraint therefore factorizes into terms which either couple only the variables $q^t$ and $q_i^s$ at fixed lattice time $i$ or couple only the variables $q^t$. One can thus express the constraint of continuity of flux in the form

$$\delta[q] \equiv \delta[q^t, q^s] = \delta^t[q^t] \prod_i \delta^i[q^t, q_i^s]. \qquad (4)$$

Finally, Wilson loop observables obey a similar decomposition. As noted above in conjunction with Eq. (2), a Wilson loop $W$ is simply given as a product over the plaquettes making up a tiling of the loop. Each of the plaquettes is determined exclusively by its dual vortex elementary square via Eq. (2); one can therefore group the product into factors as

$$W[q] \equiv W[q^t, q^s] = \prod_i W^i[q^t, q_i^s]. \qquad (5)$$

The noise reduction method given by Lüscher and Weisz operates by introducing a hierarchy into the Monte Carlo averaging of $W$ over the variables $q$, governed by the action $S$ and the constraint $\delta$, as follows:

$$\langle W \rangle_{\{q;\delta;S\}} = \frac{1}{Z} \int [Dq^t] \delta^t[q^t] \exp(-S^t[q^t])$$
$$\times \prod_i \int [Dq_i^s] \delta^i[q^t, q_i^s]$$
$$\times W^i[q^t, q_i^s] \exp(-S^i[q^t, q_i^s])$$
$$= \left\langle \prod_i \langle W^i \rangle_{\{q_i^s;\delta^i;S^i\}}[q^t] \right\rangle_{\{q;\delta;S\}}.$$

That is, one keeps the variables $q^t$ fixed while performing the inner averagings over the sets of variables $q_i^s$ according to the corresponding actions $S^i$ and constraints $\delta^i$; then, the outer expectation value over the product of these inner averages, taken over the full set of variables $q$ according to the full action $S$ and the full constraint $\delta$, may fluctuate much less than if one were simply to average the original Wilson loop $W[q]$. As noted in Sec. II, updates of the random vortex world surfaces are performed on all six surfaces of an elementary three-dimensional cube in the lattice simultaneously; in the inner averaging step, therefore, only cubes extending into three spatial directions, i.e., lying in a fixed time slice, are updated.

This algorithm can be straightforwardly iterated, i.e., further levels of averaging can be introduced in which, at each level, the quantities being averaged only depend on a subset of the variables on which the quantities at the next-lower level depended. Concretely, from the set of variables $q^t$ a further subset can be selected which is kept fixed while one averages over its complement, provided the action, the constraint and the observable can still be decomposed analogously to Eqs. (3)–(5). In the present work, one additional such iteration was performed, namely, the set of variables $q^t$ was partitioned into the sets $q_{2i}^t$ of squares
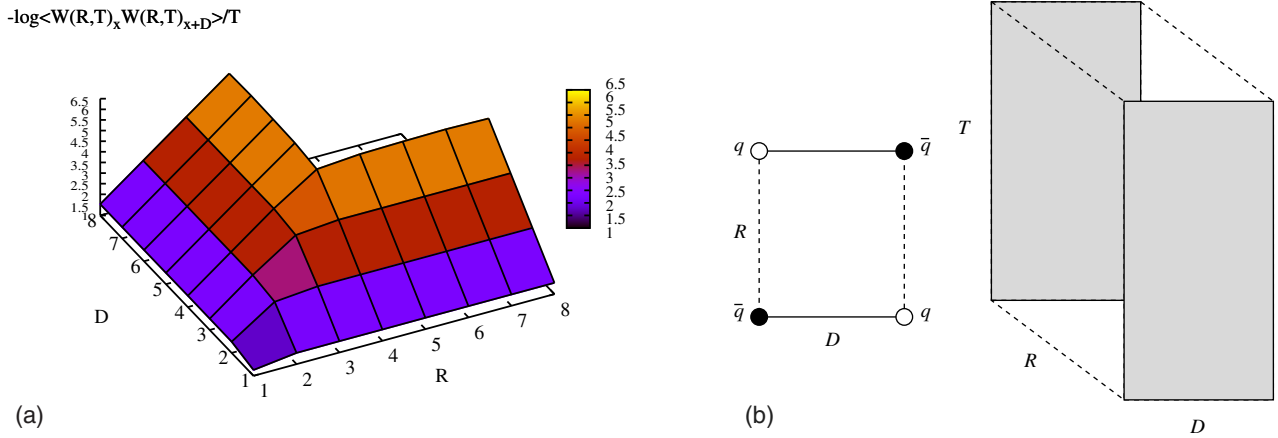
FIG. 2.  (a) $Z(2)$ static meson-meson Polyakov loop correlators $-\log\langle W(R, T=4)_x W(R, T=4)_{x+D}\rangle/T$ for various distances $R$ between quark and antiquark and distances $D$ between static mesons on $16^3 \times 4$ lattices [the $Z(3)$ results look, apart from the slightly different string tension, the same]. (b) The expectation values of the static meson-meson correlator are given by the minimal area of possible Polyakov loop combinations and display bond rearrangement between the quarks if $D < R$; compare to Fig. 1(a).

extending from lattice time $(2i-1)$ to lattice time $(2i)$, with the remaining squares constituting the set $\bar{q}^t$ which is again kept fixed at this second level in the hierarchy. This partitioning again yields decompositions of the type (3)–(5), given that for any $i$, the set of variables $q_{2i}^t$ only enters the product of inner averages

$$\langle W^{2i-1}\rangle_{q_{2i-1}^s;\delta^{2i-1};S^{2i-1}}\langle W^{2i}\rangle_{q_{2i}^s;\delta^{2i};S^{2i}}.$$

In this second level of averaging, therefore, one performs updates associated with all elementary three-dimensional lattice cubes except for the ones extending from even lattice times $2i$ to the next higher odd lattice times $2i+1$.

Finally, note that the autocorrelations between successive measurements can be practically rendered negligible by updating the full configuration a significant number of times before evaluating the next sample. This adds only a small overhead to the total execution time, which is dominated by the time required for the computation of the time-slice averages, but exponentially reduced compared to measuring the observable with the same accuracy but without the error reduction method [61].

## IV. MEASUREMENTS AND RESULTS

We measure static meson-meson and baryon-antibaryon correlators on $16^3 \times 4$ lattices, which is still well in the confinement phase; the deconfinement transition occurs between inverse temperature $T = 2$ and $T = 1$ for both $Z(2)$ and $Z(3)$ models with optimized curvature action parameters [cf. Eq. (1)], namely, $c = 0.24$ and $c = 0.21$, respectively [16,19]. The corresponding string tensions are very similar, $\sigma a^2 = 0.755$ in the $Z(2)$ case [16] and $\sigma a^2 = 0.766$ for the $Z(3)$ vortex model [21], implying a lattice spacing of about $a = 0.39$ fm in both cases if one sets the zero-temperature string tension to $\sigma = (440 \text{ MeV})^2$. In practice, it turned out to be efficient to carry out the

innermost averaging in the error reduction method by Lüscher and Weisz [61] described above using 8000 configurations; in the second-level averaging, 800 configurations were used. For the outermost averaging, typically 200 configurations were enough to achieve a sufficient level of accuracy. The correlator eventually becomes sensitive to the double-precision machine accuracy at $-\log\langle W(R, T=4)_x W(R, T=4)_{x+D}\rangle/T = 6$, i.e., for individual meson/baryon loops $\langle W(R, T=4)\rangle \approx 10^{-12}$.

### A. Static meson-meson correlator in $Z(2)$ and $Z(3)$ vortex background

We show the static meson-meson potential $-\log\langle W(R, T=4)_x W(R, T=4)_{x+D}\rangle/T$ for various quark source separations $R$ and distances $D$ between two static mesons in Fig. 3 for the $Z(2)$ case and in Fig. 4 for the $Z(3)$ vortex model. The potential is, in fact, symmetric with respect to $R$ and $D$; the plots for constants $R$ and $D$, respectively, hence lie on top of each other.[4] Once the distance $D$ between the two static mesons becomes smaller than the quark source separation within the mesons, i.e., the spatial meson loop extent $R$, we observe bond rearrangement, i.e., the chromoelectric strings will always connect quark sources such as to minimize their combined length. The potential follows a direct area law as predicted by vortex models; the bond rearrangement just means that the correlator will always measure the minimal area of possible

---

[4]It should be noted that this $R - D$ symmetry is manifest in the multiple Polyakov loop correlators which are being evaluated in the present specific calculational setup; on the other hand, for general Wilson loop correlators which do not extend over the entire temporal extent of the lattice, one would presumably have to take care to allow for sufficiently long Euclidean time evolution in order to render switching on-and-off effects, which break the symmetry, negligible, and thus recover the $R - D$ symmetry.
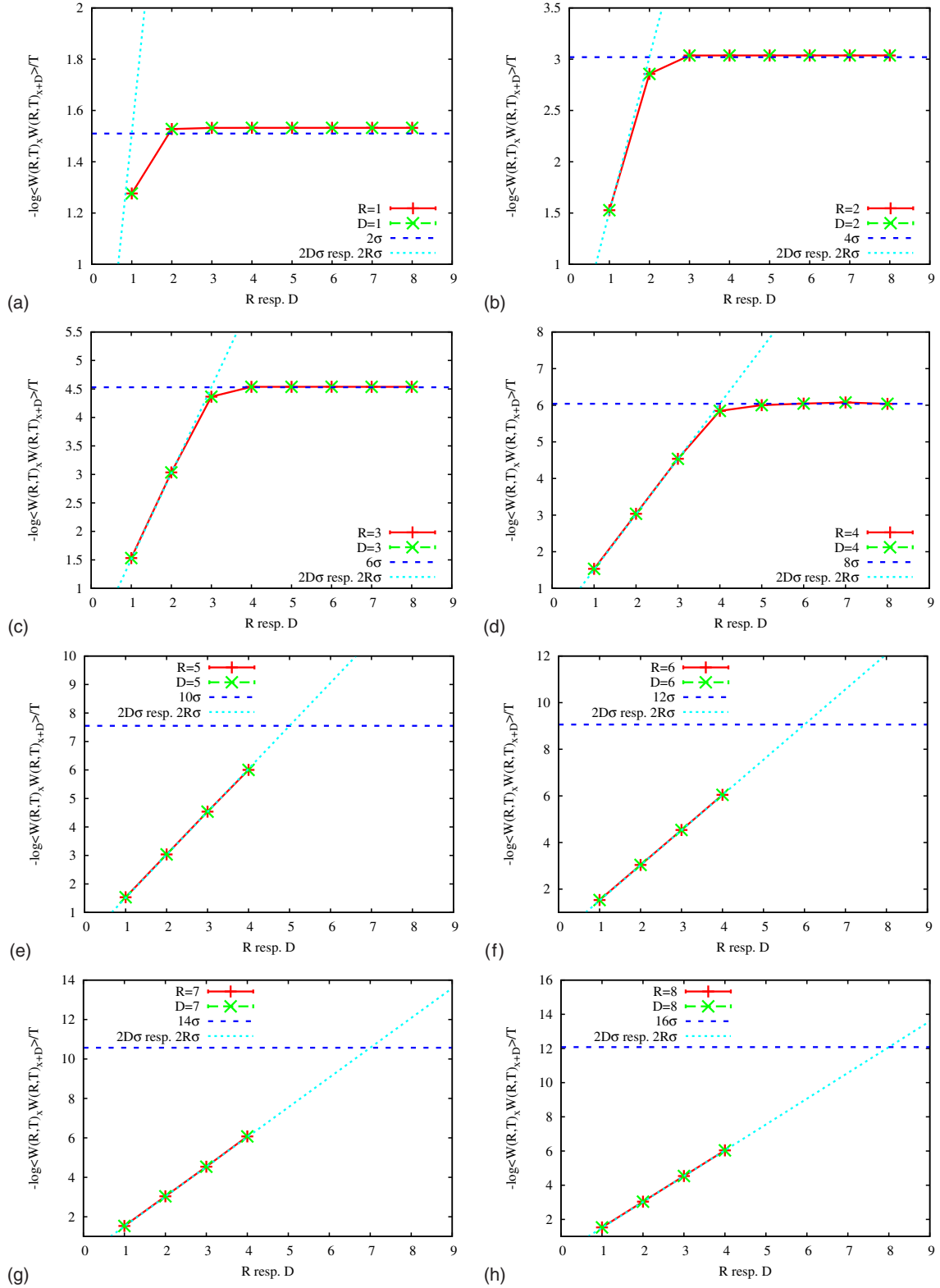
FIG. 3. $Z(2)$ static meson-meson potentials (Polyakov loop correlators) $-\log\langle W(R, T = 4)_x W(R, T = 4)_{x+D}\rangle/T$ for various distances $R$ between quark and antiquark and distances $D$ between static mesons on $16^3 \times 4$ lattices. Range of extracted lattice data is limited by machine precision.
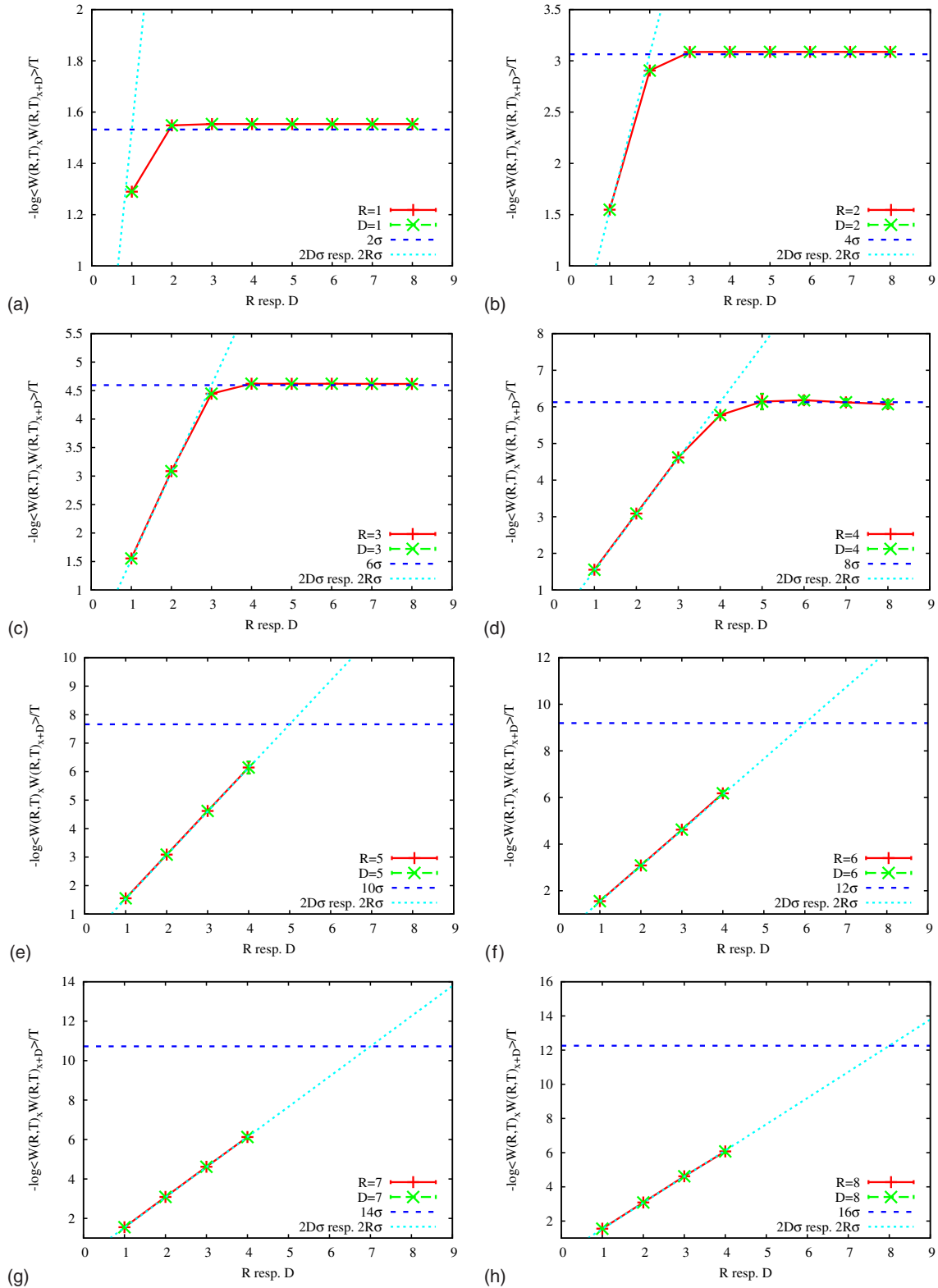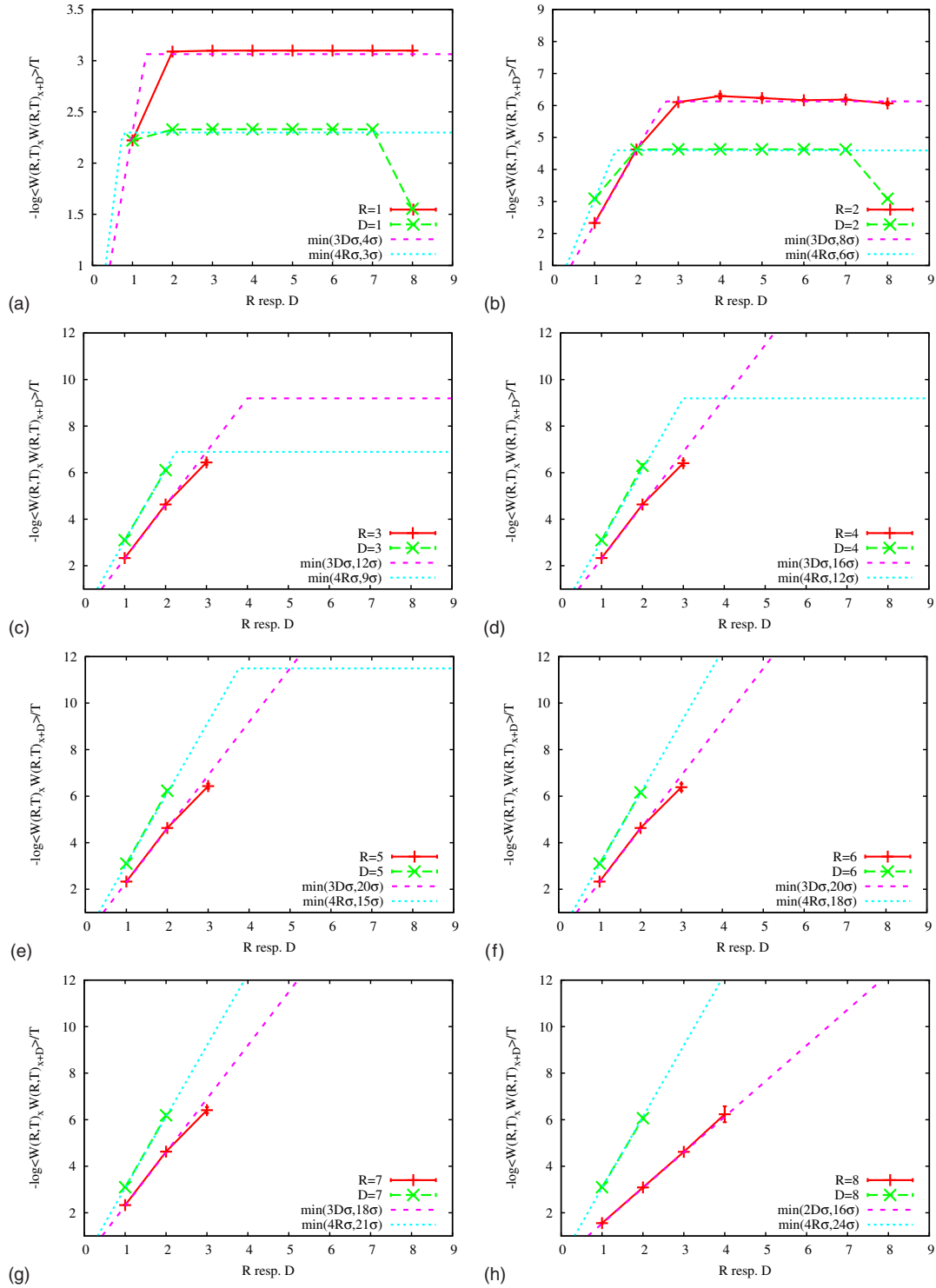
FIG. 4. $Z(3)$ static meson-meson potentials (Polyakov loop correlators) $-\log\langle W(R, T = 4)_x W(R, T = 4)_{x+D}\rangle/T$ for various distances $R$ between quark and antiquark and distances $D$ between static mesons on $16^3 \times 4$ lattices. Range of extracted lattice data is limited by machine precision.

FIG. 5. $Z(3)$ static baryon-antibaryon potentials (Polyakov loop correlators) $-\log\langle W(R, T = 4)_x W(R, T = 4)_{x+D}\rangle/T$ for various distances $R$ between quark sources within the static baryons and distances $D$ between static baryon and antibaryon on $16^3 \times 4$ lattices, compared with minimal area law predictions in cyan (short dashed lines) for constant $D$ data (green dashed lines) and in magenta (dashed lines) for constant $R$ data (red solid lines). The plateau ratios $4R\sigma : 3D\sigma$ can be understood from the Polyakov loop setup shown in Fig. 6(b); it is simply the area ratio of the Polyakov loop correlators in the $R$ vs $D$ direction. For constant $D$ plots (green dashed line), the data drop from the $3D\sigma$ plateau to $2D\sigma$ at $R = 8$ since, in this case, one is left with a static meson-meson correlator because the two outer quarks (antiquarks) of the initial static baryon (antibaryon) recombine to an antiquark (quark) source. The $R = 8$ (red solid) line in the bottom right plot (h) corresponds to the static meson-meson correlator in Fig. 4(h). Range of extracted lattice data is limited by machine precision.
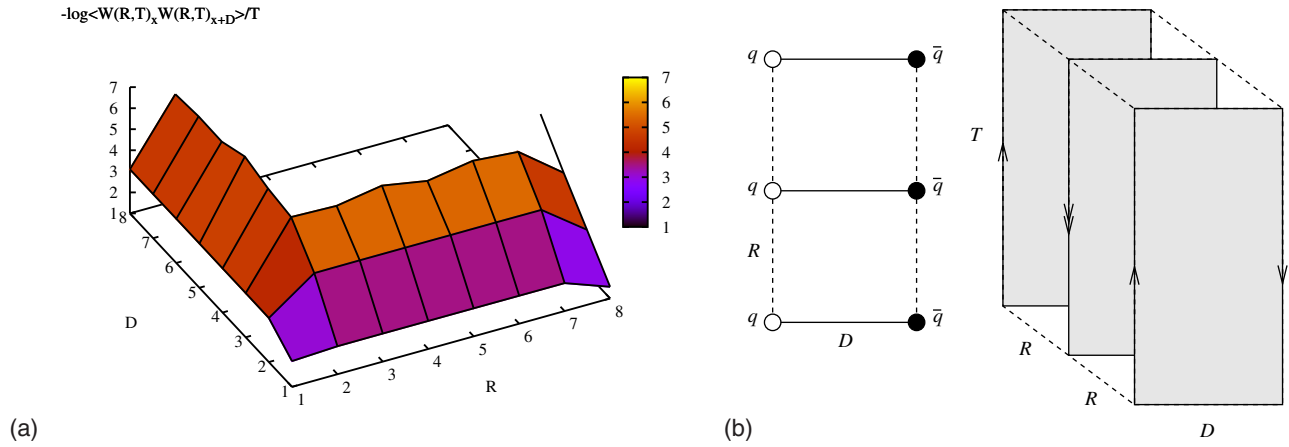
FIG. 6. (a) $Z(3)$ static baryon-antibaryon potentials (Polyakov loop correlators) $-\log\langle W(R,T)_x W(R,T)_{x+D}\rangle/T$ for various distances $R$, with $T = 4$, between quarks (or antiquarks), and distances $D$ between static baryon and antibaryon on $16^3 \times 4$ lattices. (b) Polyakov loop setup reflects the plateau ratios $4R\sigma : 3D\sigma$ in Fig. 5, i.e., 4 meson loops in $R$ direction vs 3 in $D$ direction, meaning that, if $3D < 4R$, bond rearrangement between the quark sources changes the static baryon-antibaryon into three static mesons.

Polyakov loop combinations, and its values can easily be reproduced by the form $2R\sigma$ or $2D\sigma$, respectively, indicated by blue (dashed) and cyan (short dashed) lines using the corresponding string tensions from above. As the two string tensions are almost the same, also $Z(2)$ and $Z(3)$ results are likewise, and we only show the $Z(2)$ correlator as a 3D plot in Fig. 2(a) vs $R$ and $D$, reflecting the $R - D$ symmetry, and the bond rearrangement, i.e., minimal area behavior. As long as machine precision is sufficient, i.e., up to distances $R = 4$ or $D = 4$, the potentials nicely follow the cyan (short dashed) and blue (dashed) predictions of minimal area: the potential first scales linearly with quark (meson) separation and stays constant once the active bonds are not extended anymore. At bond rearrangement regions where $R \approx D$ the data show small deviations which are most likely caused by mixed states. At small separations [cf. Figs. 3(a), 3(b), 4(a), and 4(b)], the potentials are still affected by short-distance modifications to the asymptotic linear behavior, and thus they lie slightly above the constant blue (dashed) line.

Defining the potential energy $V(R)$ to asymptotically go to zero, i.e., $V(R) = E(R) - E(\infty)$, we have to shift our potentials by their asymptotic values $2R\sigma$, i.e., the two mesonic areas, in order to compare our results with $SU(2)$ and $SU(3)$ lattice studies [62,63]. Taking into account the fixed lattice spacing $a = 0.39$ fm of the vortex models and the fact that center vortices do not reproduce Coulomb effects, the potentials are reproducing QCD results including the bond rearrangement behavior [64]; compare, for example, Figs. 4(b) and 1(b) in [63].

### B. Static baryon-antibaryon correlator in $Z(3)$ vortex background

In Figs. 5 and 6(a) we present 2D and 3D plots of static baryon-antibaryon potentials in the $Z(3)$ vortex model with respect to quark source separations $R$ and baryon

distances $D$. There is no more $R - D$ symmetry, which becomes clear in Fig. 6(b), when after bond rearrangement we do not correlate a static baryon and antibaryon anymore, but rather three static mesons. Hence, we have four mesonic loops making up the static baryon and antibaryon vs three static meson loops, and as the same minimal area law behavior as above applies, the plateau ratios $4R\sigma : 3D\sigma$ in Fig. 5 can easily be understood. A nice detail is observed for static baryons with $R = 8$ on our lattices with spatial lattice extent 16: In this case, the outer sources in the baryon and in the antibaryon, respectively, share the same spatial position and couple ($3 \otimes 3 \rightarrow \bar{3}, \bar{3} \otimes \bar{3} \rightarrow 3$), leaving a static meson-meson correlator, as is evident from the constant $D$ data (green lines, dashed) which drop at $R = 8$ from $3D\sigma$ to $2D\sigma$. Thus, the potentials again follow nicely the minimal area predictions; however, the signal becomes limited owing to machine precision limitations for $R$, respectively, $D > 2$. Nevertheless, the potential energy redefined to asymptotically go to zero, i.e., shifted by the asymptotic value $4R\sigma$ (two baryonic areas), is again in good agreement with $SU(3)$ lattice studies [65], keeping in mind the fact that center vortices do not reproduce a Coulomb potential and short distance effects cannot be studied within the vortex models at fixed lattice spacing $a = 0.39$ fm.

## V. CONCLUSIONS

Complementing earlier results within random center vortex world-surface models, which successfully describe the confinement-deconfinement transition and reproduce (spatial as well as temporal) string tensions, topological susceptibility and the (quenched) chiral condensate, we analyze static meson-meson and baryon-antibaryon potentials in $Z(2)$ and $Z(3)$ center vortex backgrounds. To this end, we calculate multiple Polyakov loop correlators corresponding to static meson-meson and baryon-antibaryon

configurations in a hypercubic lattice model of random vortex world surfaces, an effective model for the infrared sector of Yang-Mills theory. An analysis of this type, namely, of the area law associated with pairs of flat Wilson loops in a center vortex background, similar to the analysis of multiple Polyakov loop correlators performed here, had also been suggested previously in [60].

We find that the expectation values of the static meson-meson and baryon-antibaryon correlators follow a minimal area law. Bond rearrangement results when the mesons, respectively, the baryon and antibaryon become too close to one another; i.e., it becomes energetically favorable to recombine the quark sources to two, respectively, three complementary static meson pairs. No evidence of long-distance tails in the potentials, i.e., van der Waals type forces, is found as the bonded clusters are separated; the confining bonds in the clusters thus appear to be truly saturating. Cluster separation occurs already at finite distances, not only in an asymptotic sense. These properties are expected for the confining dynamics governing quarks in the strong interaction [64], and our results are in good agreement with $SU(2)$ and $SU(3)$ lattice studies [62,63,65] at long distances, keeping in mind the fact that center vortices do not reproduce a Coulomb potential, and short distance effects cannot be studied within the vortex models at fixed lattice spacing $a = 0.39$ fm. It should be emphasized that there is no conclusive *a priori* argument in favor of the (plausible) conjecture that the random vortex world-surface model exhibits this behavior, i.e., that it generates a strict minimal area law at finite separations as described above. Thus, our study constitutes a nontrivial test of the random vortex world-surface model, investigating aspects of the confining dynamics of the model which had not been previously probed. The model indeed reproduces the confinement characteristics expected within the strong interaction.

Work is in progress to investigate static meson-meson correlators in random center vortex models using quadratic and circular Wilson (not Polyakov) loop correlators, focusing on the minimal area law [66]. Motivated by the minimal surface of revolution problem, we aim to analyze possible signs of catenary solutions.

## ACKNOWLEDGMENTS

[1] G. 't Hooft, On the phase transition towards permanent quark confinement, Nucl. Phys. **B138**, 1 (1978).

[2] P. Vinciarelli, Fluxon solutions in non-abellian gauge models, Phys. Lett. **78B**, 485 (1978).

[3] T. Yoneya, Z(N) topological excitations in Yang-Mills theories: Duality and confinement, Nucl. Phys. **B144**, 195 (1978).

[4] J. M. Cornwall, Quark confinement and vortices in massive gauge-invariant QCD, Nucl. Phys. **B157**, 392 (1979).

[5] G. Mack and V. B. Petkova, Comparison of lattice gauge theories with gauge groups $Z_2$ and SU(2), Ann. Phys. (N.Y.) **123**, 442 (1979).

[6] H. B. Nielsen and P. Olesen, A quantum liquid model for the QCD vacuum: Gauge and rotational invariance of domained and quantized homogeneous color fields, Nucl. Phys. **B160**, 380 (1979).

[7] L. Del Debbio, M. Faber, J. Greensite, and Š. Olejník, Center dominance and $Z_2$ vortices in SU(2) lattice gauge theory, Phys. Rev. D **55**, 2298 (1997).

[8] K. Langfeld, H. Reinhardt, and O. Tennert, Confinement and scaling of the vortex vacuum of SU(2) lattice gauge theory, Phys. Lett. B **419**, 317 (1998).

[9] L. Del Debbio, M. Faber, J. Greensite, and Š. Olejník, Center dominance, center vortices, and confinement, arXiv:hep-lat/9708023.

[10] L. Del Debbio, M. Faber, J. Giedt, J. Greensite, and Š. Olejník, Detection of center vortices in the lattice Yang-Mills vacuum, Phys. Rev. D **58**, 094501 (1998).

[11] T. G. Kovács and E. T. Tomboulis, Vortices and confinement at weak coupling, Phys. Rev. D **57**, 4054 (1998).

[12] C. Alexandrou, M. D'Elia, and P. de Forcrand, The relevance of center vortices, Nucl. Phys. B, Proc. Suppl. **83–84**, 437 (2000).

[13] M. Engelhardt, K. Langfeld, H. Reinhardt, and O. Tennert, Deconfinement in SU(2) Yang-Mills theory as a center vortex percolation transition, Phys. Rev. D **61**, 054504 (2000).

[14] R. Bertle, M. Engelhardt, and M. Faber, Topological susceptibility of Yang-Mills center projection vortices, Phys. Rev. D **64**, 074504 (2001).

[15] R. Bertle and M. Faber, Vortices, confinement and Higgs fields, arXiv:hep-lat/0212027.

[16] M. Engelhardt and H. Reinhardt, Center vortex model for the infrared sector of Yang-Mills theory—Confinement and deconfinement, Nucl. Phys. **B585**, 591 (2000).

[17] M. Engelhardt, Center vortex model for the infrared sector of Yang–Mills theory: Topological susceptibility, Nucl. Phys. **B585,** 614 (2000).

[18] M. Engelhardt, Center vortex model for the infrared sector of Yang–Mills theory—Quenched Dirac spectrum and chiral condensate, Nucl. Phys. **B638,** 81 (2002).

[19] M. Engelhardt, M. Quandt, and H. Reinhardt, Center vortex model for the infrared sector of SU(3) Yang–Mills theory—Confinement and deconfinement, Nucl. Phys. **B685,** 227 (2004).

[20] M. Quandt, H. Reinhardt, and M. Engelhardt, Center vortex model for the infrared sector of SU(3) Yang–Mills theory: Vortex free energy, Phys. Rev. D **71,** 054026 (2005).

[21] M. Engelhardt, Center vortex model for the infrared sector of SU(3) Yang-Mills theory: Baryonic potential, Phys. Rev. D **70,** 074004 (2004).

[22] M. Engelhardt, Center vortex model for the infrared sector of SU(4) Yang-Mills theory: String tensions and deconfinement transition, Phys. Rev. D **73,** 034015 (2006).

[23] M. Engelhardt and B. Sperisen, Center vortex model for Sp(2) Yang-Mills theory, Phys. Rev. D **74,** 125011 (2006).

[24] M. Engelhardt, Center vortex model for the infrared sector of SU(3) Yang-Mills theory: Topological susceptibility, Phys. Rev. D **83,** 025015 (2011).

[25] D. Altarawneh, M. Engelhardt, and R. Höllwieser, A model of random center vortex lines in continuous $2 + 1$ dimensional space-time (to be published).

[26] R. Höllwieser, D. Altarawneh, and M. Engelhardt, Random center vortex lines in continuous 3D space-time, AIP Conf. Proc. **1701,** 030007 (2014), .

[27] L. E. Oxman, Confinement of quarks and valence gluons in SU(N) Yang-Mills-Higgs models, J. High Energy Phys. 03 (2013) 038.

[28] L. E. Oxman, BPS center vortices in nonrelativistic $SU(N)$ Gauge models with adjoint Higgs fields, arXiv:1404.2482.

[29] S. M. H. Nejad and S. Deldar, Contributions of the center vortices and vacuum domain in potentials between static sources, J. High Energy Phys. 03 (2015) 016.

[30] L. E. Oxman, BPS center vortices in nonrelativistic $SU(N)$ Gauge models with adjoint Higgs fields, Adv. High Energy Phys. **2015,** 494931 (2015).

[31] P. de Forcrand and M. D'Elia, Relevance of Center Vortices to QCD, Phys. Rev. Lett. **82,** 4582 (1999).

[32] C. Alexandrou, P. de Forcrand, and M. D'Elia, The role of center vortices in QCD, Nucl. Phys. **663A–664A,** 1031 (2000).

[33] M. Engelhardt and H. Reinhardt, Center projection vortices in continuum Yang–Mills theory, Nucl. Phys. **B567,** 249 (2000).

[34] D. B. Leinweber, P. O. Bowman, U. M. Heller, D.-J. Kusterer, K. Langfeld, and A. G. Williams, Role of centre vortices in dynamical mass generation, Nucl. Phys. B, Proc. Suppl. **161,** 130 (2006).

[35] V. G. Bornyakov, E.-M. Ilgenfritz, M. Müller-Preussker, B. V. Martemyanov, S. M. Morozov, and A. I. Veselov, Interrelation between monopoles, vortices, topological charge and chiral symmetry breaking: Analysis using overlap fermions for SU(2), Phys. Rev. D **77,** 074507 (2008).

[36] G. Jordan, R. Höllwieser, M. Faber, and U. M. Heller, Tests of the lattice index theorem, Phys. Rev. D **77,** 014515 (2008).

[37] R. Höllwieser, M. Faber, J. Greensite, U. M. Heller, and Š. Olejník, Center vortices and the Dirac spectrum, Phys. Rev. D **78,** 054508 (2008).

[38] P. O. Bowman, K. Langfeld, D. B. Leinweber, A. Sternbeck, L. von Smekal, and A. G. Williams, Role of center vortices in chiral symmetry breaking in SU(3) gauge theory, Phys. Rev. D **84,** 034501 (2011).

[39] R. Höllwieser, Center vortices and chiral symmetry breaking, Ph.D. thesis, Vienna, Technische Universität, Atominstitut 01-11-2009, http://katalog.ub.tuwien.ac.at/AC05039934.

[40] R. Höllwieser, M. Faber, and U. M. Heller, Lattice index theorem and fractional topological charge, arXiv:1005.1015.

[41] R. Höllwieser, M. Faber, and U. M. Heller, Intersections of thick center vortices, Dirac eigenmodes and fractional topological charge in SU(2) lattice gauge theory, J. High Energy Phys. 06 (2011) 052.

[42] E.-A. O'Malley, W. Kamleh, D. Leinweber, and P. Moran, SU(3) centre vortices underpin both confinement and dynamical chiral symmetry breaking, Proc. Sci., LAT2011 (2011) 257.

[43] R. Höllwieser, M. Faber, and U. M. Heller, Critical analysis of topological charge determination in the background of center vortices in SU(2) lattice gauge theory, Phys. Rev. D **86,** 014513 (2012).

[44] E.-A. O'Malley, W. Kamleh, D. Leinweber, and P. Moran, SU(3) center vortices underpin confinement and dynamical chiral symmetry breaking, Phys. Rev. D **86,** 054503 (2012).

[45] T. Schweigler, R. Höllwieser, M. Faber, and U. M. Heller, Colorful SU(2) center vortices in the continuum and on the lattice, Phys. Rev. D **87,** 054504 (2013).

[46] R. Höllwieser, T. Schweigler, M. Faber, and U. M. Heller, Center vortices and chiral symmetry breaking in SU(2) lattice gauge theory, Phys. Rev. D **88,** 114505 (2013).

[47] D. Trewartha, W. Kamleh, and D. Leinweber, Centre vortex effects on the overlap quark propagator, Proc. Sci., LATTICE2014 (2014) 357.

[48] M. Faber and R. Höllwieser, How center vortices break chiral symmetry, AIP Conf. Proc. **1701,** 030005 (2016), .

[49] N. Brambilla et al., QCD and strongly coupled gauge theories: Challenges and perspectives, Eur. Phys. J. C **74,** 2981 (2014).

[50] S. M. H. Nejad, M. Faber, and R. Höllwieser, Colorful plane vortices and chiral symmetry breaking in $SU(2)$ lattice gauge theory, J. High Energy Phys. 10 (2015) 108.

[51] D. Trewartha, W. Kamleh, and D. Leinweber, Evidence that centre vortices underpin dynamical chiral symmetry breaking in SU(3) gauge theory, Phys. Lett. B **747,** 373 (2015).

[52] D. Trewartha, W. Kamleh, and D. Leinweber, Connection between center vortices and instantons through gauge-field smoothing, Phys. Rev. D **92,** 074507 (2015).

[53] R. Höllwieser and M. Engelhardt, Smearing center vortices, Proc. Sci., LAT2014 (2014) 356.

[54] R. Höllwieser and M. Engelhardt, Approaching SU(2) gauge dynamics with smeared Z(2) vortices, Phys. Rev. D **92,** 034502 (2015).

[55] T. Banks and A. Casher, Chiral symmetry breaking in confining theories, Nucl. Phys. **B169,** 103 (1980).

[56] J. Greensite and R. Höllwieser, Double-winding Wilson loops and monopole confinement mechanisms, Phys. Rev. D **91,** 054509 (2015).

[57] J. Greensite, The confinement problem in lattice gauge theory, Prog. Part. Nucl. Phys. 51, 1 (2003).

[58] M. Engelhardt, Generation of confinement and other nonperturbative effects by infrared gluonic degrees of freedom, Nucl. Phys. B, Proc. Suppl. 140, 92 (2005).

[59] K. Holland, M. Pepe, and U. Wiese, The deconfinement phase transition of Sp(2) and Sp(3) Yang–Mills theories in (2 + 1) and (3 + 1)-dimensions, Nucl. Phys. B694, 35 (2004).

[60] J. M. Cornwall, Open issues in confinement, for the lattice and for center vortices, Proc. Sci., QCD-TNT09 (2009) 007.

[61] M. Lüscher and P. Weisz, Locality and exponential error reduction in numerical lattice gauge theory, J. High Energy Phys. 09 (2001) 010.

[62] H. R. Fiebig, H. Markum, A. Mihály, K. Rabitsch, M. Sander, and H. V. von Geramb, Meson-meson potentials from lattice QCD and inverse scattering, Acta Phys. Hung. A 22, 37 (2005).

[63] G. Bali, and M. Hetzenegger (QCDSF Collaboration), Static-light meson-meson potentials, Proc. Sci., LAT2010 (2010) 142.

[64] F. Lenz, J. T. Londergan, E. J. Moniz, R. Rosenfelder, M. Stingl, and K. Yazaki, Quark confinement and hadronic interactions, Ann. Phys. (N.Y.) 170, 65 (1986).

[65] T. Inoue (HAL QCD Collaboration), Baryon-baryon potentials in the flavor SU(3) limit from lattice QCD, Proc. Sci., LAT2009 (2009) 133.

[66] R. Höllwieser and D. Altarawneh, Center vortices, area law and the catenary solution, Int. J. Mod. Phys. A 30, 1550207 (2015).